Behavioral/Cognitive

Distinct Neurophysiological Correlates of the fMRI BOLD Signal in the Hippocampus and Neocortex

Paul F. Hill,[1] Sarah E. Seger,[2] Hye Bin Yoo,[2] Danielle R. King,[1] David X. Wang,[3] Bradley C. Lega,[2] and Michael D. Rugg[1,4]

[1]Center for Vital Longevity, University of Texas at Dallas, Dallas, Texas 75235, [2]Department of Neurosurgery, University of Texas Southwestern Medical Center, Dallas, Texas 75390, [3]Department of Electrical and Computer Engineering, Southern Methodist University, Dallas, Texas 75275, and [4]School of Psychology, University of East Anglia, Norwich NR4 7TJ, England

Functional magnetic resonance imaging (fMRI) is among the foremost methods for mapping human brain function but provides only an indirect measure of underlying neural activity. Recent findings suggest that the neurophysiological correlates of the fMRI blood oxygenation level-dependent (BOLD) signal might be regionally specific. We examined the neurophysiological correlates of the fMRI BOLD signal in the hippocampus and neocortex, where differences in neural architecture might result in a different relationship between the respective signals. Fifteen human neurosurgical patients (10 female, 5 male) implanted with depth electrodes performed a verbal free recall task while electrophysiological activity was recorded simultaneously from hippocampal and neocortical sites. The same patients subsequently performed a similar version of the task during a later fMRI session. Subsequent memory effects (SMEs) were computed for both imaging modalities as patterns of encoding-related brain activity predictive of later free recall. Linear mixed-effects modeling revealed that the relationship between BOLD and gamma-band SMEs was moderated by the lobar location of the recording site. BOLD and high gamma (70–150 Hz) SMEs positively covaried across much of the neocortex. This relationship was reversed in the hippocampus, where a negative correlation between BOLD and high gamma SMEs was evident. We also observed a negative relationship between BOLD and low gamma (30–70 Hz) SMEs in the medial temporal lobe more broadly. These results suggest that the neurophysiological correlates of the BOLD signal in the hippocampus differ from those observed in the neocortex.

Key words: **electrophysiology; episodic memory; fMRI; gamma; hippocampus; neocortex**

Significance Statement

The BOLD signal forms the basis of fMRI but provides only an indirect measure of neural activity. Task-related modulation of BOLD signals are typically equated with changes in gamma-band activity; however, relevant empirical evidence comes largely from the neocortex. We examined neurophysiological correlates of the BOLD signal in the hippocampus, where the differing neural architecture might result in a different relationship between the respective signals. We identified a positive relationship between encoding-related changes in BOLD and gamma-band activity in the frontal and parietal cortices. This effect was reversed in the hippocampus, where BOLD and gamma-band effects negatively covaried. These results suggest regional variability in the transfer function between neural activity and the BOLD signal in the hippocampus and neocortex.

Introduction

Functional magnetic resonance imaging (fMRI) is one of the foremost noninvasive methods for the examination of human brain function. However, despite the near ubiquity of fMRI in cognitive neuroscience research, the blood oxygenation level-dependent (BOLD) signal, the basis of fMRI, provides only an indirect measure of underlying neural activity. Prior studies that acquired simultaneous fMRI BOLD and intracranial electrophysiological (iEEG) recordings from primary sensory cortices of nonhuman mammals have consistently reported that stimulus-elicited BOLD signal changes are strongly correlated with changes in high frequency (>30 Hz) gamma-band activity measured in extracellular local field potentials (LFPs; Logothetis et al.,

Received Feb. 2, 2021; revised Apr. 30, 2021; accepted June 2, 2021.

Author contributions: D.R.K., B.C.L., and M.D.R. designed research; P.F.H. and D.R.K. performed research; P.F.H., S.E.S., H.B.Y., and D.X.W. analyzed the data; P.F.H., B.C.L., and M.D.R. wrote the paper.

This project was supported by the National Institute of Neurological Disorders and Stroke (Grant No. R21NS095094). We thank Arne Ekstrom for comments on the manuscript. We also thank Kay Moolenijzer, Alexa Hassien, Lisa Bagen, Eugenio Forbes, and Linley Robinson for assistance during the course of this project.

P.F. Hill's present address: Department of Psychology, University of Arizona, Tucson, Arizona 85721.

S.E. Seger's present address: Department of Neuroscience, University of Arizona, Tucson, Arizona 85721.

D.R. King's present address: Exponent, Los Angeles, California 90066.

The authors declare no competing financial interests.

Correspondence should be addressed to Paul F. Hill at paulhill@arizona.edu or Michael D. Rugg at mrugg@utdallas.edu.

https://doi.org/10.1523/JNEUROSCI.0278-21.2021

2001; Niessing et al., 2005; Goense and Logothetis, 2008). Subsequent multimodal imaging investigations in humans have largely confirmed the close relationship between changes in BOLD signal intensity and high-frequency LFPs in auditory (Nir et al., 2007), sensorimotor (Hermes et al., 2012), and association (Ojemann et al., 2010; Conner et al., 2011) cortices.

The relationship between the fMRI BOLD signal and its underlying neurophysiology has generally been assumed to be uniform across different brain regions. Recent findings challenge this assumption, however, raising questions about the possible regional specificity of coupling between BOLD and LFP signal modulations (Conner et al., 2011; Ekstrom et al., 2009; Ekstrom, 2010, 2021; Logothetis, 2008; Ojemann et al., 2013). Of particular relevance to the current study is the potential for a dissociation between the fMRI BOLD signal and the underlying neurophysiology in the hippocampus, where sparse vascularization and neural coding schemes might lead to a different relationship between the respective signals evident in the neocortex (Ekstrom, 2021). This possibility is strengthened by the very different laminar organizations that are found in the hippocampal allocortex and the neocortex, including neocortical regions adjacent to the hippocampus such as the entorhinal and parahippocampal cortices. To anticipate the present results, we observed a negative relationship between encoding-related BOLD and gamma-band activity in the hippocampus that was in stark contrast to the positive relationship between the respective signals evident in the neocortex.

In the only multimodal fMRI-iEEG study of the human medial temporal lobe (MTL) to date, Ekstrom et al. (2009) compared measures of fMRI BOLD signal with extracellular iEEG activity recorded from the hippocampus and parahippocampal gyrus in five neurosurgical patients as they performed a virtual navigation task. A positive correlation between changes in the BOLD signal and theta (4–8 Hz) activity was evident in the parahippocampal gyrus and, for microelectrodes located in regions where a significant increase in BOLD activity was also evident, in the hippocampus proper. Crucially, and in contradiction to the aforementioned findings from the sensory and association cortex, changes in high-frequency gamma activity did not correlate significantly with corresponding BOLD activity in either the hippocampus or parahippocampal gyrus. It bears mentioning, however, that these findings were based on a small sample of subjects ($n = 5$) with recordings confined to the MTL. It is therefore unclear whether the lack of correlation between BOLD and high-frequency LFPs was the result of insufficient statistical power, and whether potential BOLD-LFP coupling in the hippocampus and proximal MTL structures truly differed from that observed on the cortical surface.

In the present study, 15 patients with medically resistant temporal lobe epilepsy (TLE) implanted with depth electrodes performed a verbal delayed free recall task while iEEG was recorded simultaneously from hippocampal and neocortical sites. The same patients subsequently performed a similar version of the free recall task in a later fMRI session (Hill et al., 2020). Subsequent memory effects (SMEs) were computed from the fMRI and iEEG signals as patterns of encoding-related brain activity that were predictive of successful recall following a brief distractor interval (Paller and Wagner, 2002). The fMRI BOLD SMEs extracted from hippocampal and neocortical sites were correlated with electrophysiological SMEs obtained from the same sites. The primary aim of the study was to identify the iEEG frequency band(s) that best predicted a commensurate BOLD response, and to determine if the relationships between BOLD and iEEG SMEs varied between the hippocampus and neocortex.

Materials and Methods

Behavioral and group-level fMRI data from this experiment were the topic of a prior report (Hill et al., 2020). The present descriptions of the free recall task and behavioral results overlap heavily with the descriptions given in that report and are only summarized here. The fMRI and iEEG findings described below have not been reported previously.

Participants

Fifteen patients with medically resistant temporal lobe epilepsy were recruited to participate in this experiment (21–59 years; mean = 37 years; SD = 12 years; 10 females). Three participants were left-handed, and all spoke fluent English before the age of five. Each patient underwent iEEG to localize and monitor epileptogenic activity, during which time they performed a verbal delayed free recall task similar to the one performed during a subsequent fMRI session. The number and placement of the electrodes were determined solely on the basis of clinical considerations. Origin of epileptogenic activity was right lateralized in seven patients, left lateralized in four patients, and bilateral in the remaining four patients. Enrollment was limited to patients who correctly recalled at least 10% of study items across a full iEEG session. No patient had radiologic evidence of hippocampal sclerosis. All patients performed the iEEG session before enrollment in the fMRI version of the experiment, with an average delay of 87 d between sessions (SD = 66 d; range, 15–270 d). All patients gave informed consent in accordance with the University of Texas at Dallas and University of Texas Southwestern Institutional Review Boards and were financially compensated for their time.

Experimental Design and Statistical Analyses

Free recall task. Patients performed similar versions of a verbal delayed free recall task while undergoing iEEG recording and fMRI scanning on separate occasions. All patients completed the iEEG version of the experiment before enrolling in the fMRI study. Both versions of the recall task contained three phases: study, arithmetic distractor, and free recall (see 'fMRI Session' and 'iEEG Session' below for session specific parameters). During the study phase, participants viewed words randomly selected from a database of high-frequency concrete nouns (https://memory.psych.upenn.edu/WordPools). All words were concrete nouns between three and six letters in length, with a mean frequency per million of 46.89 (SD = 84.37; range, 0.55–557.12) obtained from the SUBTLEX-US corpus (Brysbaert and New, 2009). Concreteness ratings ranged between 3.75 and 5 (mean = 4.80; SD = 0.20) on a scale from 1 (most abstract) to 5 (most concrete; Brysbaert et al., 2014). Participants were instructed to form a mental image of the object denoted by each word and to refrain from saying the word aloud or rehearsing previously studied words. The study phase was followed by a brief arithmetic distractor task to prevent rehearsal and to clear the contents of working memory. Immediately following the distractor interval, participants were prompted to freely recall as many words from the immediately preceding study list as they could remember, in any order, for 30 s. Responses were made verbally and transcribed for subsequent analyses.

fMRI Session. Participants received instructions on the experimental tasks and performed several practice trials before entering the scanner. During the task proper, they completed a total of 18 Study-Distractor-Recall cycles divided equally over six functional scanner runs. Structural T1-weighted MPRAGE scans were collected on completion of the final block. The entire scanning session took ~65 min. During the study phase, participants viewed lists of 15 words presented sequentially in white font on a black background. The presentation of each word was preceded by a red warning fixation cross presented for 500 ms, followed by the presentation of a single word for 1800 ms. An additional seven null trials (white fixation cross) were pseudrandomly interspersed throughout each study list under the constraint that no more than three null trials occurred consecutively. This resulted in an interstimulus fixation interval that jittered between 900 and 9600 ms. Immediately following the study phase, participants performed a 15s distractor task

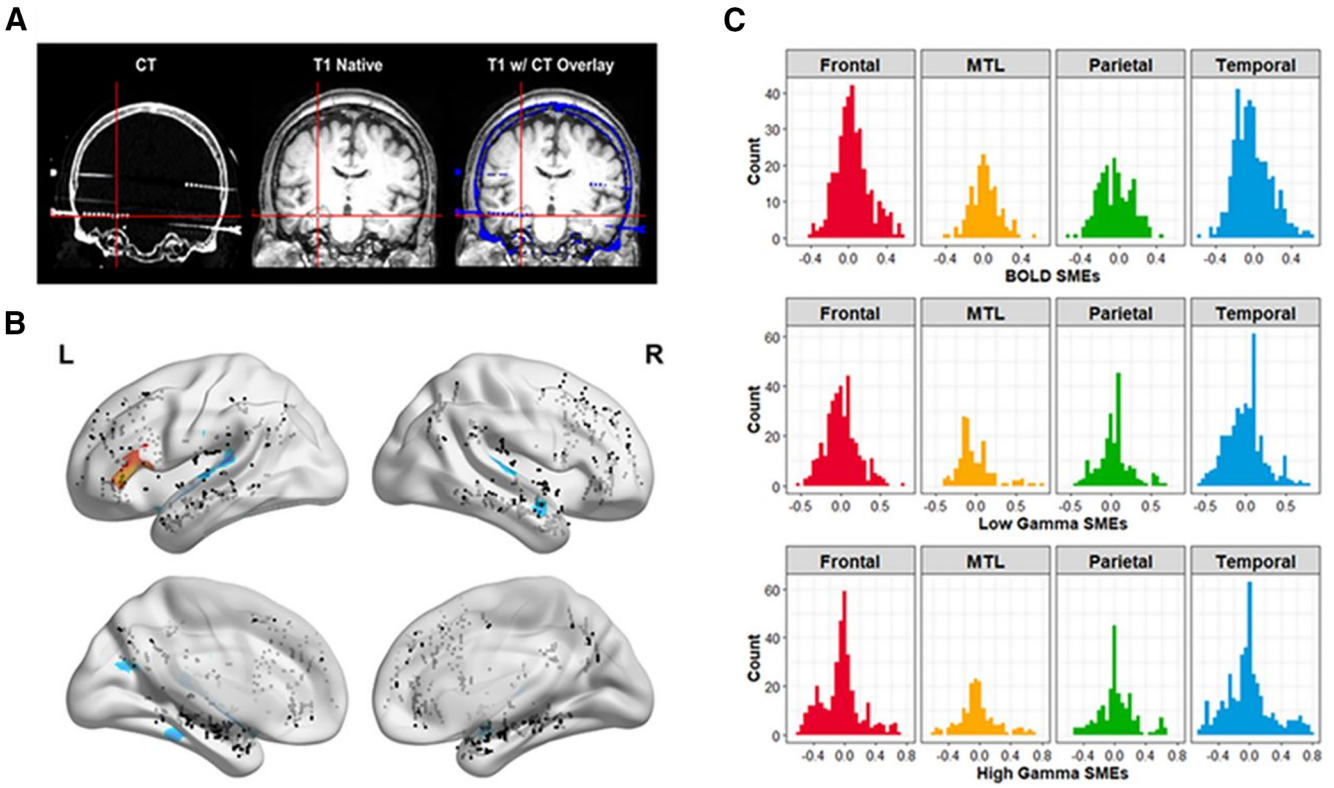

Figure 1. ***A***, Example of a hippocampal contact localized on a coregistered native computed tomography (CT, left) and T1 (middle) image. Note that the left and middle views are for illustrative purposes only. The CT image was overlaid on the T1 image (right, CT overlay shown in blue) so that contacts could be manually localized with reference to stereotaxic coordinates in standard MNI space. ***B***, ROI coverage superimposed on the outcome of the group-level fMRI recalled versus not recalled contrast (for illustrative purposes, liberally thresholded at $p < 0.01$ uncorrected, 30 contiguous voxels). Warm and cool colors reflect positive and negative SMEs, respectively. ***C***, Histograms color coded by lobe showing the across-ROI distribution of BOLD (top), low gamma (middle), and high gamma (bottom) SMEs. Values on the *y*-axis reflect the standardized SMEs.

involving simple arithmetic problems in the form of A + B = C? Participants were tasked with indicating whether the expression was correct or incorrect via a button press using their right index and middle fingers (counterbalanced across participants). Each expression remained on the screen until a response was made, with the instruction that responses should be made quickly and accurately. Verbal responses during the free recall phase were recorded for later transcription using a scanner-compatible microphone (Optoacoustics) and noise-cancelling software (OptiMRI version 3.2) to filter out scanner noise.

iEEG Session. All patients performed a version of the free recall task similar to that described above for the MRI session with the following differences. Patients performed 26 Study-Distractor-Recall cycles per session (the first of these being for practice and not included in the analyses). Seven of 15 patients completed more than one session (mean number of sessions = 3; range, 2–7), with multiple sessions per patient occurring on average 2 d apart. The task was performed on a laptop computer during an inpatient hospital stay following intracranial electrode placement. Study lists were composed of 12 concrete nouns selected at random without replacement. Four patients completed a protocol that included 10 items per study list; for these subjects the analyzed data came from an experiment that included brain stimulation, but only lists in which all items were presented and recalled in the absence of stimulation (nonstimulation lists) were included in the analyses. Each word was presented for 1800 ms followed by a random interitem fixation jitter (750–1000 ms). Following each study list, patients performed a 20 s arithmetic distractor task comprising expressions in the form of A + B + C = ? Patients were required to enter a response to each expression via the keyboard. The free recall phase was identical to that described for the MRI session.

MRI data acquisition and preprocessing

Functional and anatomic images were acquired with a Philips 3.0T Achieva MRI scanner equipped with a 32-channel receiver head coil. Functional images were acquired using a T2*-weighted, BOLD echoplanar imaging (EPI) sequence (sensitivity encoding [SENSE] factor 2, flip angle 70°, 80 × 78 matrix, field of view [FOV] = 24 cm, repetition time [TR] = 2000 ms, and echo time [TE] = 30 ms). EPI volumes consisted of 34 slices (1 mm interslice gap) with a voxel size of 3 × 3 × 3 mm. Slices were acquired in ascending order oriented parallel to the anterior commissure–posterior commissure line. Each functional run included 201 EPI volumes. T1-weighted anatomic images were acquired with a magnetization-prepared rapid gradient echo pulse sequence (FOV = 240 × 240, 1 × 1 × 1 mm isotropic voxels, 34 slices, sagittal acquisition). Participants performed a total of 18 study-test cycles split evenly into six scanner runs.

All fMRI preprocessing and analyses were conducted with Statistical Parametric Mapping (SPM12; Wellcome Centre for Human Neuroimaging), run under MATLAB R2017a (MathWorks). Functional images were realigned to the mean EPI image and slice-time corrected using sinc interpolation to the 17th slice. The images were then reoriented and spatially smoothed with an isotropic 8 mm full-width half-maximum Gaussian kernel. The data from the six scanning runs were concatenated using the spm_fmri_concatenate function. All analyses reported below were performed in native space on smoothed data.

MRI data analysis

A separate single-trial general linear model (GLM) was constructed for each participant. Note that group-level effects were reported previously by Hill et al. (2020) and are summarized in Figure 1*B*. Data from the six study sessions were concatenated and subjected to a least squares all GLM (Rissman et al., 2004; Mumford et al., 2014) to estimate the BOLD response for each trial separately. Each study event was modeled with a delta function convolved with the canonical hemodynamic response function. Six regressors representing motion-related variance (three for rigid-body translation and three for rotation) and six session-specific regressors were included in each model as covariates of no interest.

For each region of interest (ROI; see below, ROI localization), we extracted parameter estimates for the single-trial BOLD responses, averaged across all voxels falling within a given ROI. Single-trial BOLD values were used to compute SMEs as the standardized mean difference between subsequently recalled (R) and not recalled (NR) study items using the following formula:

$$\mathrm{SME} = \frac{\mu_R - \mu_{NR}}{\sqrt{\frac{\sigma_R^2 + \sigma_{NR}^2}{2}}}.$$

In the above formula, μ_R and σ^2_R refer to the across trial mean and variance of BOLD activity for subsequently recalled study items, respectively, and μ_{NR} and σ^2_{NR} refer to the across trial mean and variance of BOLD activity for subsequently forgotten study items. This formula produces SME values for each ROI that are akin to a Cohen's *d* effect size estimate. Positive values thus reflect regions where increased brain activity was predictive of subsequent remembering (so-called positive subsequent memory effects), and negative values reflect regions where a relative increase in brain activity is predictive of subsequent forgetting (so-called negative subsequent memory effects). It is important to note, the metric is insensitive to individual differences in the gain of the hemodynamic transfer function that mediates between neural activity and the associated BOLD signal.

iEEG data acquisition and preprocessing

Stereo-EEG data were recorded with a Nihon Kohden EEG-1200 clinical system. Each electrode contained 8–12 contacts spaced 2–4 mm apart. Signals were sampled at 1000 Hz and referenced to a common intracranial contact. Raw signals were subsequently rereferenced to the median white-matter signal computed separately for each subject. All analyses were conducted using MATLAB with proprietary and custom-made scripts. We employed kurtosis-based artifact rejection with a threshold of <5 to exclude interictal activity and abnormal trials (Sederberg et al., 2006). The raw signals were filtered for line noise and the first harmonic on a session-by-session basis using a first-order bandstop Butterworth filter with a stopband from 58 to 62 Hz and from 118 to 122 Hz.

iEEG data analysis

To compute spectral power, we convolved the median white-matter rereferenced EEG with 53 complex valued Morlet wavelets (width 6 cycles) spaced logarithmically from 2 to 150 Hz. The magnitude of the wavelet transform was then squared and log transformed to yield instantaneous power. Power estimates for each electrode were *z*-scored separately for each frequency bin using the mean and SD of the power estimate from the 200 ms prestimulus baseline interval. Normalized power was then averaged within six canonical frequency ands: delta (2–4 Hz), theta (4–8 Hz), alpha (8–12 Hz), beta (12–30 Hz), low gamma (30–70 Hz), and high gamma (70–150 Hz). SMEs were computed over the entire 1800 ms epoch during which the study item was presented using the same formula used to compute BOLD SMEs (see above). For subsidiary analyses, additional SMEs were computed separately for early (0–900 ms) and late (900–1800 ms) epochs.

Theta/gamma phase-amplitude coupling

To compute phase-amplitude coupling (PAC), we used the Hilbert transform to extract instantaneous phase and power information for theta (4–8 Hz), low gamma (30–70 Hz), and high gamma (70–150 Hz) frequency bands over the entire 1800 ms encoding epoch. These frequency bands were selected a priori and were motivated by previous observations that theta/gamma PAC is associated with successful memory encoding in the hippocampus and neocortex (Lega et al., 2016; Wang et al., 2021). To identify PAC, we used the phase of the theta frequency (Φ_{f1}, phase-modulating frequency) and the amplitude of the relevant gamma-band frequency (A_{f2}, amplitude-modulated frequency) employing the methods previously described by Wang et al. (2021; but see also Canolty et al., 2006). For each contact, single-trial estimates of PAC were contrasted according to subsequent memory status (R versus NR) using the same approach as that employed to generate BOLD and iEEG power SMEs.

Table 1. Mean number of ROIs (with range) per subject in each of the four lobar regions

Region	Mean (range) number ROIs
Frontal	24 (3–55)
Temporal (non-MTL)	26 (9–37)
Parietal	14 (2–32)
MTL	11 (4–22)

ROI localization

Intracranial contacts were localized using postimplant computed tomography (CT) and structural T1 MR scans. CT images were linearly coregistered to the T1 MRI obtained during the fMRI session using Functional MRI of the Brain (FMRIB) Software Library (FSL) Linear Image Registration Tool (FLIRT version 6.0.1; Jenkinson and Smith, 2001; Jenkinson et al., 2002, 2012; Greve and Fischl, 2009). For each participant, the native T1 image was then loaded into MRIcron stereotaxic space and overlaid with the coregistered native CT image. As illustrated in Figure 1*A*, microelectrode contacts were visible as high-intensity artifacts on the CT overlay. Contacts were manually localized with reference to stereotaxic coordinates in standard Montreal Neurological Institute (MNI) space for each patient.

Each patient's native mean functional T2* image was manually inspected to ensure adequate alignment with the native T1 image. To eliminate contacts affected by signal dropout and distortions caused by susceptibility artifacts, we loaded the mean T2* image into MRIcron and visually inspected the coordinates for each contact to ensure adequate signal quality. Contacts falling within areas affected by magnetic susceptibility artifact were flagged and excluded from subsequent analyses. This procedure identified a total of 139 contacts (10%) for exclusion.

To identify contacts located in white matter, tissue segmentation of the structural T1 scans was performed using FMRIB Automated Segmentation Tool in FSL (Zhang et al., 2001) with white-matter pattern probability set at 70%. Contacts visible on the CT overlay were manually inspected with reference to the white-matter mask, and those falling within the mask in all three stereotaxic directions (*x*, *y*, *z*) were labeled as white-matter contacts. For each subject, these white-matter contacts were combined to provide a grand median reference signal that was used to compute SMEs (see above, iEEG data analysis). We note that the criteria for selecting white-matter contacts were more conservative than those for localizing gray-matter contacts, ensuring that the white-matter reference signal was unlikely to include any residual signal from gray matter. Contacts located outside the skull were flagged and excluded from further analyses, as were all gray-matter contacts showing evidence of ictal activity or other pathology.

For the fMRI analyses, spherical ROIs (3 mm radius) were generated using the MarsBaR (version 0.44) toolbox for SPM. Each ROI was centered on the native stereotaxic coordinates corresponding to the gray-matter contacts localized in the aforementioned paragraphs. The mean fMRI BOLD SME was then computed across all voxels falling within each sphere using the procedures described (see above, MRI data analysis). Note that rerunning each of the principal analyses described below on BOLD estimates extracted from single voxel ROIs (cf. Ojemann et al., 2010) yielded highly comparable results.

Each contact was labeled by a trained neuroradiologist according to the Automated Anatomical Labeling (AAL) atlas (Tzourio-Mazoyer et al., 2002). For quality assurance, all hippocampal- and parahippocampal-labeled contacts were also manually inspected and their locations confirmed by the first author. The AAL labels were used to sort ROIs into lobar and sublobar parcels in the region-based analyses reported below. The mean number of ROIs for each patient per lobe are reported in Table 1.

Statistical analyses

Statistical analyses were conducted using R software (https://www.r-project.org/). ANOVAs were conducted using the afex package (https://CRAN.R-project.org/package=afex), and the Greenhouse-Geisser procedure (Greenhouse and Geisser, 1959) was used to correct degrees of

Table 2. Comparison of nested random effects

Frequency	χ^2	*p* value	ΔAIC
Delta	22.56	4.99^{-5}	17
Theta	23.15	3.75^{-5}	17
Alpha	24.20	2.66^{-5}	18
Beta	21.57	8.03^{-5}	16
Low gamma	46.18	5.20^{-10}	40
High gamma	29.42	1.83^{-6}	23

AIC, Akaike information criterion.

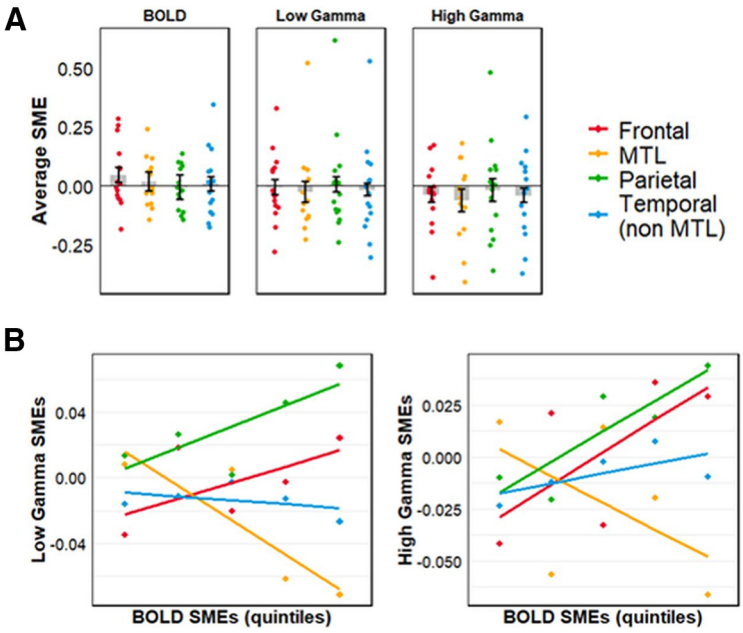

Figure 2. ***A***, Plots showing the average BOLD and gamma-band SMEs for each lobe. Each dot reflects the average SME for a single patient. Error bars reflect the across-subject SE of the mean. ***B***, Scatterplots showing the relationship between BOLD and gamma-band subsequent memory effects in the MTL and neocortex. Left, A significant negative relationship between BOLD and low gamma SMEs was evident in the MTL. The relationship between BOLD and low gamma SMEs in frontal, temporal, and parietal cortex was not significant. Right, A significant positive relationship between BOLD and high gamma SMEs was evident in frontal and parietal cortex. These effects were accompanied by a negative but nonsignificant relationship between BOLD and high gamma SMEs in the MTL. Data are binned into quintiles based on the magnitude of BOLD SMEs for visualization purposes.

freedom for nonsphericity when necessary. *Post hoc* tests on significant effects from the ANOVAs were conducted using the emmeans package (https://CRAN.R-project.org/package=emmeans). Multiple regression and correlation analyses were performed using the lm and cor.test functions in the base R package, respectively. Linear mixed-effects (LME) models were performed using the lme4 package (Bates et al., 2015), and degrees of freedom were estimated using the Kenward-Roger method. A 95% confidence interval for fixed effects was computed via parametric bootstrapping in the broom.mixed package (https://cran.r-project.org/package=broom.mixed). All models included a random intercept per subject. Inclusion of additional random intercept and slope terms are described in the relevant sections below. All models were fit using maximum likelihood Laplace approximation, and were refit using restricted maximum likelihood before performing nested model comparisons.

Results

Behavioral results

Behavioral results from the fMRI session were previously reported (Hill et al., 2020). The proportion of freely recalled study items from the fMRI session (mean = 0.30, SD = 0.11) closely approximated performance during the iEEG session (mean = 0.27, SD = 0.09). However, the iEEG session always preceded the fMRI session (see above, Materials and Methods). Given the consequent possibility of order effects, and the slight methodological differences between the free recall paradigms administered during the respective sessions (see above, Materials and Methods), we did not perform a direct statistical test to compare recall performance between the two testing sessions.

Coupling between BOLD and LFP SMEs varies across brain regions and frequency bands

In the first set of analyses, we examined whether variance in the magnitude of memory-related BOLD signal change could be predicted by variance in memory-related iEEG changes measured from the same anatomic locations and whether the relationship between BOLD and iEEG effects varied across brain regions. Each ROI was assigned to one of four lobar labels: frontal, temporal, parietal, and medial temporal (including hippocampus, parahippocampal gyrus, and amygdala). Because of sparse coverage, data extracted from ROIs in the occipital lobe (derived from a total of only eight contacts) were not included in these analyses. For each subject, the across-ROI vector of BOLD SMEs from each of the four lobar regions was entered into the model as the dependent variable. The iEEG SMEs recorded from the same ROIs in each frequency band were entered as the fixed effect of interest, along with hemisphere of ictal onset (right, left, bilateral) and handedness (left, right) as nuisance regressors. Using the lobar labels provided for each ROI, region- and subject-wise intercept and slope terms were entered into the respective LME models as fully crossed random effects.

Using nested maximum likelihood ratio tests, we found that compared with the models with only the subject-level random effects factor, inclusion of the regional random effects significantly improved model fit in each of the six frequency bands (Table 2). These results suggest that the magnitude and/or direction of the relationships between BOLD and iEEG SMEs are regionally variant. Motivated by these findings we specified an additional set of subsidiary LME models separately for each lobar region. Because the number of ROIs per lobe in any given subject was highly variable (Table 1), we elected to perform subject-wise intercept-only models (i.e., random intercepts, fixed slopes). The models were otherwise specified as before. Note that modeling the relationship between BOLD and iEEG effects at the level of sublobar cortical and subcortical loci (loci here referring to the AAL labels assigned to each ROI) did not explain any additional variance over and above the lobar models (cf. Conner et al., 2011). We therefore report below only the results of the LME models corresponding to each lobar region.

The results of the low and high gamma LME analyses are illustrated in Figure 2 and described in Table 3. BOLD SMEs positively covaried with high gamma SMEs in frontal (β = 0.14, t = 2.97; 95% CI 0.04, 0.24) and parietal (β = 0.14, t = 2.29; 95% CI = 0.02, 0.26) cortices. BOLD SMEs in the MTL negatively covaried with low gamma SMEs (β = −0.17, t = −2.62; 95% CI = −0.29, −0.05). Note that each of these effects remained

significant after controlling for the iEEG SMEs in all other frequency bands. Thus, gamma-band power changes explained unique sources of variance in encoding-related BOLD signal change in the neocortex and MTL. BOLD SMEs negatively covaried with theta SMEs in frontal lobe ($\beta = -0.13$, $t = -2.52$; 95% CI = −0.23, −0.03) and positively with alpha SMEs in the parietal lobe ($\beta = 0.21$, $t = 3.15$; 95% CI = 0.07, 0.35). When controlling for iEEG SMEs in all other frequency bands, only the negative BOLD-theta relationship in the frontal lobe remained significant.

Table 3. Parameter estimates (with SE) for each of the lobar linear mixed-effects analyses

Frequency	Frontal	MTL	Parietal	Temporal
Delta	0.06 (0.05)	−0.07 (0.08)	0.12 (0.07)	−0.06 (0.05)
Theta	**−0.13 (0.05)**	0.01 (0.09)	0.11 (0.06)	−0.01 (0.05)
Alpha	0.00 (0.05)	0.02 (0.07)	**0.21 (0.07)**	0.06 (0.05)
Beta	0.03 (0.05)	-0.06 (0.09)	0.09 (0.08)	0.03 (0.06)
Low gamma	0.06 (0.04)	**−0.17 (0.06)**	0.11 (0.07)	0.01 (0.05)
High gamma	**0.14 (0.05)**	−0.08 (0.06)	**0.14 (0.06)**	0.05 (0.04)

Significant effects are indicated by bold.

Relationship between BOLD and gamma-band SMEs in the hippocampus and parahippocampal gyrus

We next performed a set of subsidiary linear regression analyses to examine whether the relationship between BOLD and iEEG SMEs recorded from the MTL differed between parahippocampal neocortex and hippocampal allocortex (see above, Introduction). Because of sparse coverage, data extracted from ROIs in the amygdala (derived from a total of only 13 contacts from five patients) were not included in these analyses. BOLD SMEs were entered as the dependent variable, and iEEG SMEs, region, and the iEEG x region interaction terms were entered as predictor variables along with the hemisphere of ictal onset and handedness as nuisance regressors. The number of ROIs localized to the hippocampus (mean = 6; range, 0–15) and parahippocampal gyrus (mean = 5; range, 2–8) was highly variable across subjects. We therefore elected to run linear regression rather than LME analyses as the error term in the latter can be biased in cases with too few observations per random effect (in this case subject). We note that although these analyses are limited in that ROIs, rather than subjects, are treated as a random effect, a separate set of by-subject LME analyses produced identical results. Thus, for parsimony we report only the results of the linear regression analyses.

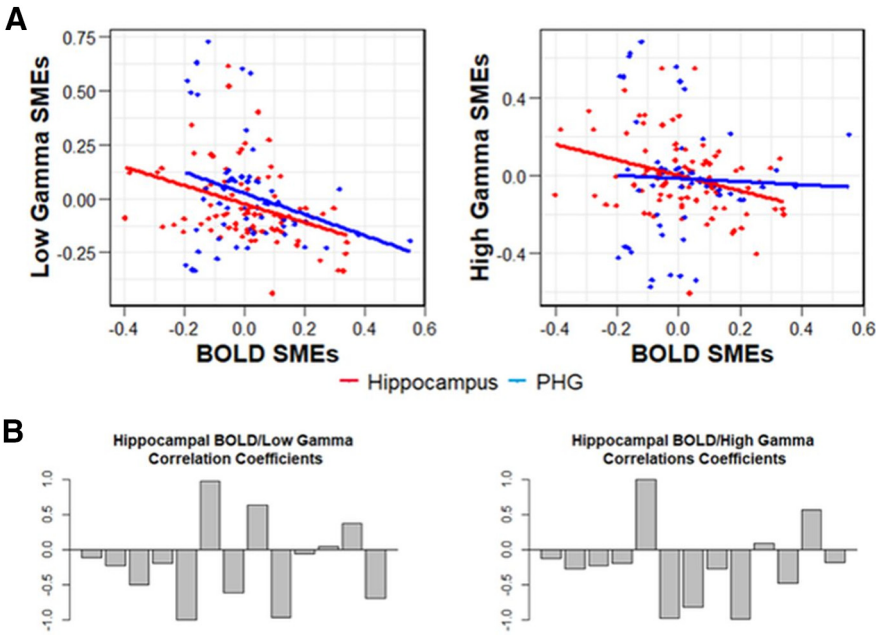

Figure 3. ***A***, Scatter plots illustrating the relationship between BOLD and gamma-band SMEs in the hippocampus and parahippocampal gyrus (PHG). Left, A significant negative correlation between BOLD and low gamma SMEs was evident in both the hippocampus and parahippocampal gyrus, and the magnitude of these correlations did not differ between the two regions. Right, A significant negative correlation between BOLD and high gamma SMEs was evident in the hippocampus, accompanied by a nonsignificant correlation between BOLD and high gamma in the parahippocampal gyrus. ***B***, For illustrative purposes, bar plots showing individual correlation coefficients between hippocampal BOLD and gamma-band SMEs are shown for each participant. Coefficients for two participants with only one or no hippocampal ROIs are not included.

The results of the low and high gamma regression analyses are illustrated in Figure 3. The analysis of high gamma effects revealed a significant interaction between region and high gamma SMEs ($F_{(1,155)} = 4.78$, $p = 0.031$), which was driven by a negative relationship between BOLD and high gamma SMEs in the hippocampus ($r = -0.32$, $p = 0.002$) and a nonsignificant relationship in the parahippocampal gyrus ($r = -0.04$, $p = 0.770$). Regression models for the remaining frequency bands failed to identify any significant region x iEEG interactions (all ps > 0.1). Consistent with the results of the MTL LME analysis reported above, the low gamma model revealed a significant main effect of iEEG ($F_{(1,159)} = 16.69$, $p < 0.001$), such that BOLD SMEs negatively covaried with low gamma SMEs recorded from the hippocampus ($r = -0.37$, $p < 0.001$) and parahippocampal gyrus ($r = -0.29$, $p = 0.029$).

We performed a set of follow-up multiple regression analyses with BOLD SMEs as the dependent variable, and the relevant gamma-band iEEG SME (low, high), ROI hemisphere, and the iEEG x ROI hemisphere interaction term as predictor variables, along with handedness and hemisphere of ictal onset as nuisance regressors. These analyses revealed nonsignificant interactions between hemisphere and the respective gamma-band effects (low, high) in the hippocampus and parahippocampal gyrus (ps > 0.1). We thus found no evidence that the relationship between BOLD and gamma-band activity in the MTL was moderated by hemisphere.

Motivated by evidence of long-axis functional specialization of the hippocampus (Hrybouski et al., 2019; Poppenk et al., 2013; Strange et al., 2014), we next assessed whether the relationship between BOLD and gamma-band SMEs differed between anterior and posterior hippocampal subregions. To this aim, each hippocampal ROI was assigned an anterior ($n = 57$) or posterior ($n = 30$) label with reference to the uncal apex. We then performed multiple regression analyses separately for the low and high gamma effects. In each model, BOLD SMEs were entered as the dependent variable, and the relevant gamma-band iEEG SME, longitudinal subregion (anterior, posterior), and the iEEG x subregion interaction term were entered as predictor variables, along with handedness and hemisphere of ictal onset as nuisance regressors. These analyses revealed nonsignificant interactions between hippocampal subregion and both low gamma ($F_{(1,86)} = 0.27$, $p = 0.603$) and high gamma ($F_{(1,86)} = 0.01$, $p = 0.915$) SMEs.

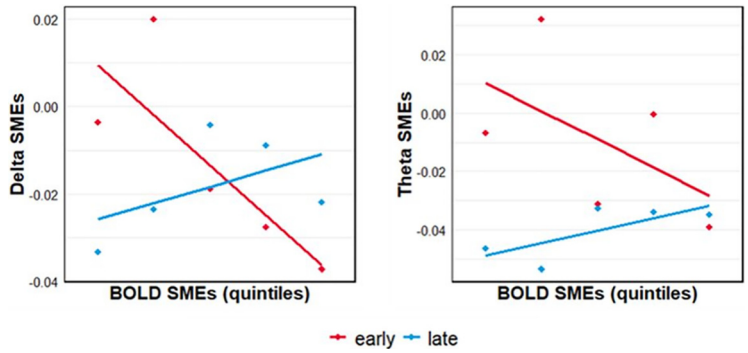

Figure 4. Scatter plots showing the relationship between BOLD and low-frequency iEEG. SMEs are moderated by epoch (early, late) in the frontal cortex. Data are binned into quintiles based on the magnitude of BOLD SMEs for visualization purposes.

Coupling between memory-related BOLD and iEEG activity in the MTL and parietal cortex is moderated by the direction of BOLD effect

As illustrated in Figure 1*C*, a distribution of both positive and negative BOLD and gamma-band SMEs were evident in each lobe. In a follow-up set of linear mixed-effects analyses, we included direction of the BOLD effect (positive, negative) as a categorical fixed effect, along with the BOLD direction x gamma-band SME interaction terms. The models were otherwise specified as previously reported. These analyses thus allowed us to assess whether the direction of BOLD effects moderated the relationship between encoding-related BOLD and gamma-band activity (cf. Ekstrom et al., 2009). They revealed a significant interaction between direction and low gamma in the MTL ($F_{(1,150.89)} = 13.96$, $p < 0.001$) and parietal lobe ($F_{(1,188.80)} = 8.63$, $p = 0.004$). *Post hoc* LME analyses revealed that coupling between BOLD and low gamma SMEs was strongest when restricted to ROIs showing a positive BOLD effect, with a significant negative relationship evident in the MTL ($\beta = -0.27$, $p < 0.001$) and a positive but nonsignificant relationship in the parietal lobe ($\beta = 0.11$, p 0.069). Effects in both regions were weaker and nonsignificant when restricted to ROIs showing a negative BOLD effect (MTL: $\beta = 0.02$, $p = 0.985$; parietal: $\beta = -0.04$, $p = 0.481$). The direction x low gamma interactions in frontal and temporal lobe were nonsignificant, as was also the case for the interactions involving high gamma SMEs.

Frontal BOLD effects are differentially predicted by early and late components of delta- and theta-band activity

In the foregoing analyses, iEEG SMEs were computed over the entire 1800 ms encoding period during which a study word was displayed. Although this roughly approximated the sampling rate of fMRI volume acquisition (2000 ms), it risks collapsing across meaningful temporal variation in the electrophysiological effects. Therefore, we examined whether the relationship between BOLD and iEEG effects differed when iEEG SMEs were estimated for early (0–900) and late (900–1800) encoding epochs. We specified LME models separately for each lobar location using an approach similar to that described in previous sections. For each subject, the across-ROI vector of BOLD SMEs from a given lobar region was entered into the model as the dependent variable. Early and late iEEG effects, epoch (early, late), and the iEEG x epoch interaction were entered as fixed effects of interest, along with handedness and hemisphere of ictal onset as nuisance regressors. Subject-wise intercepts were entered as a random effect (i.e., random intercepts, fixed slopes). Given our a priori interest in hippocampal effects, we also performed linear regression analyses on hippocampal BOLD and iEEG SMEs separately for each frequency band. For the multiple regression analyses, BOLD SMEs were entered into each respective model as the dependent variable, and iEEG SMEs, epoch, and the iEEG x epoch interaction term were entered as predictor variables along with handedness and hemisphere of ictal onset as covariates of no interest.

Modeling the relationship between BOLD and iEEG effects in the frontal cortex revealed significant interactions between epoch and low-frequency SMEs in both the delta ($F_{(1,695.79)} = 8.60$, $p = 0.003$) and theta ($F_{(1,694.59)} = 6.32$, $p = 0.012$) frequency bands (Fig. 4). *Post hoc* analyses of the delta-band effects revealed a significant positive relationship between BOLD and delta SMEs during the late epoch ($\beta = 0.19$, $t = 3.84$; 95% CI = 0.09, 0.29), along with a negative but nonsignificant relationship during the early epoch ($\beta = -0.06$, $t = -1.32$; 95% CI = −0.15, 0.03). By contrast, *post hoc* analyses of the theta-band effects revealed a significant negative relationship between BOLD and theta SMEs during the early epoch ($\beta = -0.18$, $t = -3.67$; 95% CI = −0.27, −0.08), along with a positive but nonsignificant relationship during the late epoch ($\beta = 0.07$, $t = 1.21$; 95% CI = −0.04, 0.17). The early and late temporal epochs did not moderate the relationship between BOLD and iEEG effects in any of the remaining lobar models (all ps > 0.08). Nor did we observe any evidence that epoch moderated the relationship between BOLD and iEEG effects in the hippocampus (all ps > 0.4).

Theta-to-gamma phase amplitude coupling predicts unique variance in neocortical BOLD SMEs

In a final set of analyses, we examined whether the strength of coupling between the phase of low frequency theta activity and the amplitude of high frequency gamma activity [i.e., phase-amplitude coupling (PAC)] predicted variance in encoding-related BOLD activity over and above iEEG power SMEs (cf. Murta et al., 2017). Trial-wise estimates of theta/low gamma and theta/high gamma PAC were computed for each ROI. PAC estimates for recalled and nonrecalled study items were contrasted using the same approach as that used to compute fMRI BOLD and iEEG power SMEs. This procedure thus yielded a single estimate for each contact reflecting the extent to which subsequent memory status modulated the strength of theta/gamma PAC. For each subject, the resultant across-ROI vector of BOLD SMEs collapsed across the four lobar regions was entered into LME analyses as the fixed effect of interest to predict BOLD SMEs while simultaneously controlling for theta- and gamma-band power SMEs. As before, handedness and hemisphere of ictal onset were included as nuisance regressors. Lobar- and subject-wise slope and intercept terms were entered into the respective low gamma and high gamma LME models as fully crossed random effects.

Using nested maximum likelihood ratio tests, we found that compared with the models with only the subject-level random effects factor, inclusion of the regional random effects significantly improved model fit for theta/low gamma PAC ($X^2 = 20.37$, $p < 0.001$) and theta/high gamma PAC ($X^2 = 33.81$, $p < 0.001$). Accordingly, we performed follow-up LME analyses separately for each lobe. The resultant fixed effect regression coefficients and confidence intervals are reported in Table 4. Encoding-related theta/low gamma PAC negatively

Table 4. Parameter estimates (with SE) for each of the lobar linear mixed-effects PAC analyses

Fixed Effect	Frontal	MTL	Parietal	Temporal
Theta/Low gamma				
PAC SME	−0.01 (0.04)	−0.02 (0.08)	**−0.14 (0.06)**	**−0.12 (0.05)**
theta power	**−0.13 (0.05)**	0.07 (0.09)	0.07 (0.07)	0.00 (0.05)
low gamma power	0.08 (0.04)	**−0.16 (0.06)**	0.10 (0.08)	−0.02 (0.06)
Theta/High gamma				
PAC SME	**−0.16 (0.04)**	−0.01 (0.07)	0.07 (0.07)	0.07 (0.05)
theta power	**−0.16 (0.05)**	0.01 (0.09)	0.05 (0.06)	−0.07 (0.05)
high gamma power	**0.14 (0.04)**	−0.04 (0.05)	**0.24 (0.05)**	**0.13 (0.04)**

Significant effects are indicated by bold.

covaried with BOLD SMEs in the parietal and temporal lobes. A similar negative relationship was evident in the frontal lobes, but for theta/high gamma PAC. Importantly, each of the significant relationships between encoding-related PAC and BOLD activity remained significant when controlling for theta- and gamma-band power SMEs. Theta/gamma PAC therefore explained unique variance in encoding-related BOLD activity.

In contrast to the aforementioned PAC effects observed in frontal, parietal, and temporal regions, the relationship between encoding-related BOLD and theta/gamma PAC was not significant in the MTL. Follow-up multiple regression analyses on BOLD SMEs recorded from MTL ROIs revealed non significant PAC x region interactions ($ps > 0.4$), confirming that the relationship between theta/gamma PAC and BOLD SMEs did not reliably differ between the hippocampal allocortex and parahippocampal neocortex.

Discussion

We examined whether encoding-related differences in electrophysiological activity could predict analogous differences in fMRI BOLD signal magnitude and whether any such relationships between these neurophysiological and hemodynamic signals varied according to region. BOLD and high gamma SMEs positively covaried across much of the neocortex, with reliable relationships evident in the frontal and parietal cortices. Notably, this relationship was reversed in the hippocampus, where a negative correlation between BOLD and high gamma SMEs was evident. We also observed a negative relationship between BOLD and low gamma SMEs in the MTL more broadly. Below, we discuss the significance of these findings in respect of regional variability in the transfer function between neural activity and the fMRI BOLD signal.

As just noted, using the subsequent memory procedure (Paller and Wagner, 2002) we identified robust coupling between encoding-related modulation of high gamma and BOLD activity in the frontal and parietal cortices. The relationship between BOLD and high gamma SMEs did not vary at the level of sublobar cortical loci. These findings are notable for two reasons. First, the regionally invariant relationship between BOLD and high gamma effects across much of the neocortex observed in the present study is consistent with numerous prior reports of preferential coupling between BOLD and high-frequency iEEG activity measured from the primary sensory, motor, and association cortex in behaving humans (Nir et al., 2007; Ojemann et al., 2010; Conner et al., 2011; Hermes et al., 2012). Second, the present findings replicate and extend these prior studies by establishing a link between modulation of BOLD and high-frequency iEEG activity during a memory encoding task.

In stark contrast to the robust positive relationships observed across much of the neocortex, we identified a negative relationship between BOLD and both low and high gamma SMEs in the hippocampus. Moreover, the negative relationship between BOLD and high gamma SMEs observed in the hippocampus was dissociable from the relationship evident in anatomically proximal MTL neocortex. These findings are consistent with the proposal that regional variability in patterns of coupling between BOLD and high gamma SMEs reflect regional differences in neurovascular coupling, specifically, between the hippocampus and neocortex (Ekstrom, 2021). Sparse coding and vascularization schemes might have explained the existence of a null relationship between BOLD and gamma-band iEEGs in the hippocampus relative to the neocortex (should that have been observed), but such factors cannot readily account for the reliable negative relationships that were actually observed for both low and high gamma effects in the present study. Sparse firing of principal cells in the hippocampus (particularly in dentate gyrus and CA3) is made possible by dense recurrent inhibitory interneurons that promote pattern separation (McNaughton and Morris, 1987; Yassa and Stark, 2011). Because inhibition is metabolically costly, it may be that it is these signals that were responsible for heightened hippocampal BOLD responses, while simultaneously down-regulating high frequency iEEG signals. Although speculative, this account is consistent with our observation that the relationship between hippocampal BOLD and low gamma activity was specific to ROIs showing a positive BOLD effect (cf. Ekstrom et al., 2009). This account might also explain why variation in the firing of sparsely distributed principal neurons in the hippocampus can seemingly be associated with the robust hippocampal BOLD effects that are evident across a variety of behavioral tasks such as memory encoding and retrieval (Spaniol et al., 2009; Kim, 2011) and spatial navigation (Doeller et al., 2008).

BOLD SMEs in the hippocampus negatively covaried with both low and high gamma SMEs recorded from the same locations. We note that these findings are consistent with those reported by Ekstrom et al. (2009) wherein BOLD activity in the hippocampus showed a trending negative correlation with low and high gamma activity despite using a very different behavioral paradigm (Ekstrom et al., 2009, their Fig. 4*D*,*G*). Low gamma effects in the present study remained significant when controlling for concurrent high gamma SMEs (Although the high gamma effect was rendered nonsignificant when controlling for concurrent low gamma effects.). This functional dissociation between BOLD coupling with low and high gamma is consistent with prior research reporting that low and high gamma LFPs are distinct in both their neurophysiological correlates (Buzsáki and Wang, 2012; Colgin et al., 2009; Ray and Maunsell, 2011) and their functional significance (Colgin and Moser, 2010; Bieri et al., 2014; Colgin, 2015). The present findings thus extend much of the rodent work to humans while providing novel evidence for unique low and high gamma components to the hippocampal BOLD signal. We remain agnostic, however, about the neurophysiological significance of these effects and acknowledge that future work is needed to elucidate whether low and high gamma effects do indeed reflect distinct neural correlates of the hippocampal BOLD signal.

Theta/gamma PAC has been identified as a key neurophysiological correlate of successful memory encoding (Lega et al., 2016; Wang et al., 2021) and has been posited as a potential unique source of variance in hippocampal BOLD activity (Kunz

et al., 2019). Here, we identified a negative relationship between encoding-related theta/gamma PAC and BOLD activity in the frontal, temporal, and parietal cortex. Importantly, PAC explained variance in BOLD activity over and above that explained by theta- and gamma-band power alone. This pattern of results is consistent with findings reported by Murta et al. (2017) in which beta/gamma PAC was observed to negatively covary with BOLD activity in the motor cortex during a finger-tapping task. We did not, however, observe any significant relationship between the strength of encoding-related PAC and BOLD activity in the MTL or hippocampus proper. It is not immediately clear why the relationship between BOLD and theta/gamma PAC did not extend to the hippocampus. One possibility is that PAC in the hippocampus reflects a more nuanced interaction among theta oscillations at different frequency ranges within the hippocampus, as demonstrated recently by Kota et al. (2020). Previous work also suggests that distinct frequencies underlie hippocampal-cortical cross-regional PAC (Wang et al., 2021), raising the possibility that measures of cross-regional PAC may converge more closely with fMRI measures of functional connectivity.

In the frontal cortex, BOLD SMEs were related to low-frequency delta and theta SMEs, and for each frequency band, this relationship was moderated by encoding epoch (early vs late). As illustrated in Figure 4, both delta- and theta-band effects were characterized by a negative relationship with BOLD during the early epoch, accompanied by a modest positive relationship during the later epoch (Although the reliability of these effects differed as a function of frequency band and epoch.). We note that because these results were unanticipated, they should be interpreted cautiously and are clearly in need of replication.

Because of safety considerations, simultaneous iEEG and fMRI recordings are not readily obtainable in humans. We therefore obtained electrophysiological and hemodynamic recordings from the same individuals in sequential experimental sessions, raising the possibility that order or practice effects may have confounded behavioral performance during the fMRI session. Another potential limitation of the present study concerns the methodological differences between the free recall paradigms employed during the fMRI and iEEG sessions. The lengths of the study lists and the timing of the item encoding and distractor intervals varied between the respective iEEG and fMRI sessions. Variability in each of these task parameters has been shown to influence free recall performance (Murdock, 1962; Roberts, 1972; Ward, 2002). Although we are encouraged by the similar behavioral performance observed during the fMRI and iEEG versions of the task, we are unable to definitively rule out the possibility that these task discrepancies affected the relationship between the two classes of SME.

Experimental applications of iEEG are currently limited to patients with medically refractory epilepsy, introducing potential constraints on the generalizability of intracerebral findings. Leveraging the noninvasiveness provided by fMRI, we recently reported that group-level BOLD SMEs in the same TLE patient cohort described here did not reliably differ from the SMEs observed in an age-matched neurologically healthy control group (Hill et al., 2020). Thus, neuropathology associated with TLE was apparently insufficient to give rise to detectable differences in the functional neuroanatomy of episodic memory encoding as this is reflected by the fMRI BOLD signal. These findings do not, however, rule out the possibility that coupling between electrophysiological and BOLD effects might be altered by disease status. Unfortunately, this issue cannot be resolved using within-subjects designs owing to the invasiveness of iEEG.

In conclusion, we identified a robust positive relationship between encoding-related BOLD and high gamma activity in the frontal and parietal cortex, replicating findings from numerous prior studies (Ekstrom, 2021; Ojemann et al., 2013). It is important to note that this relationship was reversed in the hippocampus, where BOLD SMEs negatively covaried with both low and high gamma SMEs. Future research will be required to address the interesting question of whether these findings vary at the level of hippocampal subfields. Nonetheless, the present results suggest that the neurophysiological correlates of the BOLD signal in the hippocampus differ from those in the neocortex.

References

Bates D, Mächler M, Bolker B, Walker S (2015) Fitting linear mixed-effects models using lme4. J Stat Soft 67:1–48.

Bieri KW, Bobbitt KN, Colgin LL (2014) Slow and fast gamma rhythms coordinate different spatial coding modes in hippocampal place cells. Neuron 82:670–681.

Brysbaert M, New B (2009) Moving beyond Kucera and Francis: a critical evaluation of current word frequency norms and the introduction of a new and improved word frequency measure for American English. Behav Res Methods 41:977–990.

Brysbaert M, Warriner AB, Kuperman V (2014) Concreteness ratings for 40 thousand generally known English word lemmas. Behav Res 46:904–911.

Buzsáki G, Wang X-J (2012) Mechanisms of gamma oscillations. Annu Rev Neurosci 35:203–225.

Canolty RT, Edwards E, Dalal SS, Soltani M, Nagarajan SS, Kirsch HE, Berger MS, Barbaro NM, Knight RT (2006) High gamma power is phase-locked to theta oscillations in human neocortex. Science 313:1626–1628.

Colgin LL (2015) Do slow and fast gamma rhythms correspond to distinct functional states in the hippocampal network? Brain Res 1621:309–315.

Colgin LL, Moser EI (2010) Gamma oscillations in the hippocampus. Physiology (Bethesda) 25:319–329.

Colgin LL, Denninger T, Fyhn M, Hafting T, Bonnevie T, Jensen O, Moser M-B, Moser EI (2009) Frequency of gamma oscillations routes flow of information in the hippocampus. Nature 462:353–357.

Conner CR, Ellmore TM, Pieters TA, DiSano MA, Tandon N (2011) Variability of the relationship between electrophysiology and BOLD-fMRI across cortical regions in humans. J Neurosci 31:12855–12865.

Doeller CF, King JA, Burgess N (2008) Parallel striatal and hippocampal systems for landmarks and boundaries in spatial memory. Proc Natl Acad Sci U S A 105:5915–5920.

Ekstrom A (2010) How and when the fMRI BOLD signal relates to underlying neural activity: the danger in dissociation. Brain Res Reviews 62:233–244.

Ekstrom AD (2021) Regional variation in neurovascular coupling and why we still lack a Rosetta Stone. Philos Trans R Soc Lond B Biol Sci 376:20190634.

Ekstrom A, Suthana N, Millett D, Fried I, Bookheimer S (2009) Correlation between BOLD fMRI and theta-band local field potentials in the human hippocampal area. J Neurophysiol 101:2668–2678.

Goense JBM, Logothetis NK (2008) Neurophysiology of the BOLD fMRI signal in awake monkeys. Curr Biol 18:631–640.

Greenhouse SW, Geisser S (1959) On methods in the analysis of profile data. Psychometrika 24:95–112.

Greve DN, Fischl B (2009) Accurate and robust brain image alignment using boundary-based registration. Neuroimage 48:63–72.

Hermes D, Miller KJ, Vansteensel MJ, Aarnoutse EJ, Leijten FSS, Ramsey NF (2012) Neurophysiologic correlates of fMRI in human motor cortex. Hum Brain Mapp 33:1689–1699.

Hill PF, King DR, Lega BC, Rugg MD (2020) Comparison of fMRI correlates of successful episodic memory encoding in temporal lobe epilepsy patients and healthy controls. Neuroimage 207:116397.

Hrybouski S, MacGillivray M, Huang Y, Madan CR, Carter R, Seres P, Malykhin NV (2019) Involvement of hippocampal subfields and anterior-posterior subregions in encoding and retrieval of item, spatial, and associative memories: Longitudinal versus transverse axis. NeuroImage 191:568–586.

Jenkinson M, Smith S (2001) A global optimisation method for robust affine registration of brain images. Med Image Anal 5:143–156.

Jenkinson M, Bannister P, Brady M, Smith S (2002) Improved optimization for the robust and accurate linear registration and motion correction of brain images. Neuroimage 17:825–841.

Jenkinson M, Beckmann CF, Behrens TEJ, Woolrich MW, Smith SM (2012) FSL. Neuroimage 62:782–790.

Kim H (2011) Neural activity that predicts subsequent memory and forgetting: a meta-analysis of 74 fMRI studies. Neuroimage 54:2446–2461.

Kota S, Rugg MD, Lega BC (2020) Hippocampal theta oscillations support successful associative memory formation. J Neurosci 40:9507–9518.

Kunz L, Maidenbaum S, Chen D, Wang L, Jacobs J, Axmacher N (2019) Mesoscopic neural representations in spatial navigation. Trends Cogn Sci 23:615–630.

Lega B, Burke J, Jacobs J, Kahana MJ (2016) Slow-theta-to-gamma phase–amplitude coupling in human hippocampus supports the formation of new episodic memories. Cereb Cortex 26:268–278.

Logothetis NK (2008) What we can do and what we cannot do with fMRI. Nature 453:869–878.

Logothetis NK, Pauls J, Augath M, Trinath T, Oeltermann A (2001) Neurophysiological investigation of the basis of the fMRI signal. Nature 412:150–157.

McNaughton BL, Morris RGM (1987) Hippocampal synaptic enhancement and information storage within a distributed memory system. Trends Neurosci 10:408–415.

Mumford JA, Davis T, Poldrack RA (2014) The impact of study design on pattern estimation for single-trial multivariate pattern analysis. Neuroimage 103:130–138.

Murdock BB (1962) The serial position effect of free recall. J Exp Psychol 64:482–488.

Murta T, Chaudhary UJ, Tierney TM, Dias A, Leite M, Carmichael DW, Figueiredo P, Lemieux L (2017) Phase-amplitude coupling and the BOLD signal: a simultaneous intracranial EEG (icEEG)—fMRI study in humans performing a finger-tapping task. Neuroimage 146:438–451.

Niessing J, Ebisch B, Schmidt KE, Niessing M, Singer W, Galuske RAW (2005) Hemodynamic signals correlate tightly with synchronized gamma oscillations. Science 309:948–951.

Nir Y, Fisch L, Mukamel R, Gelbard-Sagiv H, Arieli A, Fried I, Malach R (2007) Coupling between neuronal firing rate, gamma LFP, and BOLD fMRI is related to interneuronal correlations. Curr Biol 17:1275–1285.

Ojemann GA, Corina DP, Corrigan N, Schoenfield-McNeill J, Poliakov A, Zamora L, Zanos S (2010) Neuronal correlates of functional magnetic resonance imaging in human temporal cortex. Brain 133:46–59.

Ojemann GA, Ojemann J, Ramsey NF (2013) Relation between functional magnetic resonance imaging (fMRI) and single neuron, local field potential (LFP) and electrocorticography (ECoG) activity in human cortex. Front Hum Neurosci 7:34.

Paller KA, Wagner AD (2002) Observing the transformation of experience into memory. Trends Cogn Sci 6:93–102.

Poppenk J, Evensmoen HR, Moscovitch M, Nadel L (2013) Long-axis specialization of the human hippocampus. Trends in Cognitive Sciences 17:230–240.

Ray S, Maunsell JHR (2011) Different origins of gamma rhythm and high-gamma activity in macaque visual cortex. PLoS Biology 9:e1000610.

Rissman J, Gazzaley A, D'Esposito M (2004) Measuring functional connectivity during distinct stages of a cognitive task. Neuroimage 23:752–763.

Roberts WA (1972) Free recall of word lists varying in length and rate of presentation: a test of total-time hypotheses. J Exp Psychol 92:365–372.

Sederberg PB, Gauthier LV, Terushkin V, Miller JF, Barnathan JA, Kahana MJ (2006) Oscillatory correlates of the primacy effect in episodic memory. Neuroimage 32:1422–1431.

Spaniol J, Davidson PSR, Kim ASN, Han H, Moscovitch M, Grady CL (2009) Event-related fMRI studies of episodic encoding and retrieval: meta-analyses using activation likelihood estimation. Neuropsychologia 47:1765–1779.

Strange BA, Witter MP, Lein ES, Moser EI (2014) Functional organization of the hippocampal longitudinal axis. Nature Reviews Neuroscience 15:655–669.

Tzourio-Mazoyer N, Landeau B, Papathanassiou D, Crivello F, Etard O, Delcroix N, Mazoyer B, Joliot M (2002) Automated anatomical labeling of activations in SPM using a macroscopic anatomical parcellation of the MNI MRI single-subject brain. Neuroimage 15:273–289.

Wang DX, Schmitt K, Seger S, Davila CE, Lega BC (2021) Cross-regional phase amplitude coupling supports the encoding of episodic memories. Hippocampus 31:481–492.

Ward G (2002) A recency-based account of the list length effect in free recall. Mem Cognit 30:885–892.

Yassa MA, Stark CEL (2011) Pattern separation in the hippocampus. Trends Neurosci 34:515–525.

Zhang Y, Brady M, Smith S (2001) Segmentation of brain MR images through a hidden Markov random field model and the expectation-maximization algorithm. IEEE Trans Med Imaging 20:45–57.